ChemPhysChem

Research Article
doi.org/10.1002/cphc.202400298

Chemistry Europe
European Chemical Societies Publishing

www.chemphyschem.org

Disentangling the Conformational Space and Structural Preferences of Tetrahydrofurfuryl Alcohol Using Rotational Spectroscopy and Computational Chemistry

Weslley G. D. P. Silva[a] and Jennifer van Wijngaarden*[b]

The influence of the hydroxymethyl (CH_2OH) group on the tetrahydrofuran (THF) ring structure was investigated by disentangling the gas phase conformational landscape of the sugar analogue tetrahydrofurfuryl alcohol (THFA). By combining rotational spectroscopy (6–20 GHz) and quantum chemical calculations, transitions corresponding to two stable conformers of THFA and their ^{13}C isotopologues were observed and assigned in the rotational spectrum. The positions of the C atoms were precisely determined to unambiguously distinguish between nearly isoenergetic pairs of conformers that differ in their ring configurations: *envelope* (E) versus *twist* (T). The rotational spectrum confirms that the *E* ring geometry is favoured when the CH_2OH fragment lies *gauche* (−) to the THF backbone (OCCO ~−60°) whereas the *T* form is more stable for the *gauche* (+) alignment of the substituent (OCCO ~+60°). The observed spectral intensities suggest that conformational relaxation of the THF geometry (*E*↔*T*) to the more stable form readily occurs within the pairs of *g*− and *g*+ conformers which is consistent with the low barriers (1.5–1.7 kJ mol^{-1}) for conversion determined via transition state calculations. Insights into the intramolecular hydrogen bonding and other weak interactions stabilizing the lowest energy structures of THFA were derived and rationalized using non-covalent interaction analyses.

Introduction

Tetrahydrofurfuryl alcohol (THFA) is a sugar analog of the deoxyribose unit of DNA and RNA.[1,2] THFA (Figure 1) is chiral and its structure is composed of a pentose unit (C_4H_8O, tetrahydrofuran, THF) with a hydroxymethyl (CH_2OH) substituent on the α-carbon. The THF backbone itself is nonplanar and has been the subject of extensive molecular spectroscopic and theoretical investigations to characterize the underlying potential that governs its geometry and dynamics.[3–8] Using rotational spectroscopy, Engerholm *et al.*[8] suggested that THF has four energetically equivalent minima structures with *envelope* (*E*) ring conformations $E_\alpha/E_{\alpha'}$ and $E^\alpha/E^{\alpha'}$ (one of the α-carbons is puckered up or down while the remaining four atoms of the ring backbone are coplanar). These isoenergetic minima are interconnected by two pairs of non-equivalent maxima ${}^{\beta}T_{\beta'}/{}^{\beta'}T_{\beta}$ (twist ring structures where one β-carbon is puckered up and the other down while the α-carbons and the oxygen atom are coplanar) and E^O/E_O (oxygen atom puckered up or down while all carbons are coplanar). In the rotational spectrum of THF, a single set of transitions was observed for the ground state and showed splittings associated with a low frequency pseudorotation motion (50 cm^{-1}) between the equivalent minima. The study of Engerholm *et al.*[8] was later confirmed by Meyer *et al.*[6] who applied a flexible model to understand the observed tunneling splitting. Following this, new potential energy surfaces for THF have been reported in which i) *T* conformations;[3,7] or where ii) the pair of equivalent E^O and E_O geometries are the global minima.[4]

Although there is no consensus about the molecular structures and underlying potential energy surface of THF yet, it is of interest to investigate how the conformation of the THF ring and barriers to pseudorotation vary in the presence of different organic substituents. Xie et al[9] investigated the rotational spectrum of tetrahydro-2-furoic acid and observed that the presence of a carboxylic acid COOH substituent on THF breaks the symmetry of the ring and exclusively favours low energy conformers with *E* ring structures. This was supported by the observation of three *E* conformers in the supersonic jet. For THFA with a CH_2OH group, a previous gas phase electron diffraction study[10] reported two conformers stabilized by an intramolecular hydrogen bond and concluded that both had *T* ring structures. On the other hand, using quantum mechanical calculations and IR spectroscopy, Wang *et al.*[11] suggested that an *E* structure is favoured in the gas phase but that there are other low-lying *E* and *T* forms with similar spectral signatures.[2,11,12] Together, these reports highlight the need for further study of the conformational equilibrium of THFA using an experimental technique that is extremely sensitive to individual conformer geometries.

[a] *W. G. D. P. Silva*
I. Physikalisches Institut, Universität zu Köln, Zülpicher Str. 77, 50937 Köln, Germany

[b] *J. van Wijngaarden*
Department of Chemistry, York University, M3J 1P3 Toronto, Ontario, Canada
E-mail: vanwijng@yorku.ca

Supporting information for this article is available on the WWW under https://doi.org/10.1002/cphc.202400298

Research Article
doi.org/10.1002/cphc.202400298
Chemistry Europe
European Chemical Societies Publishing

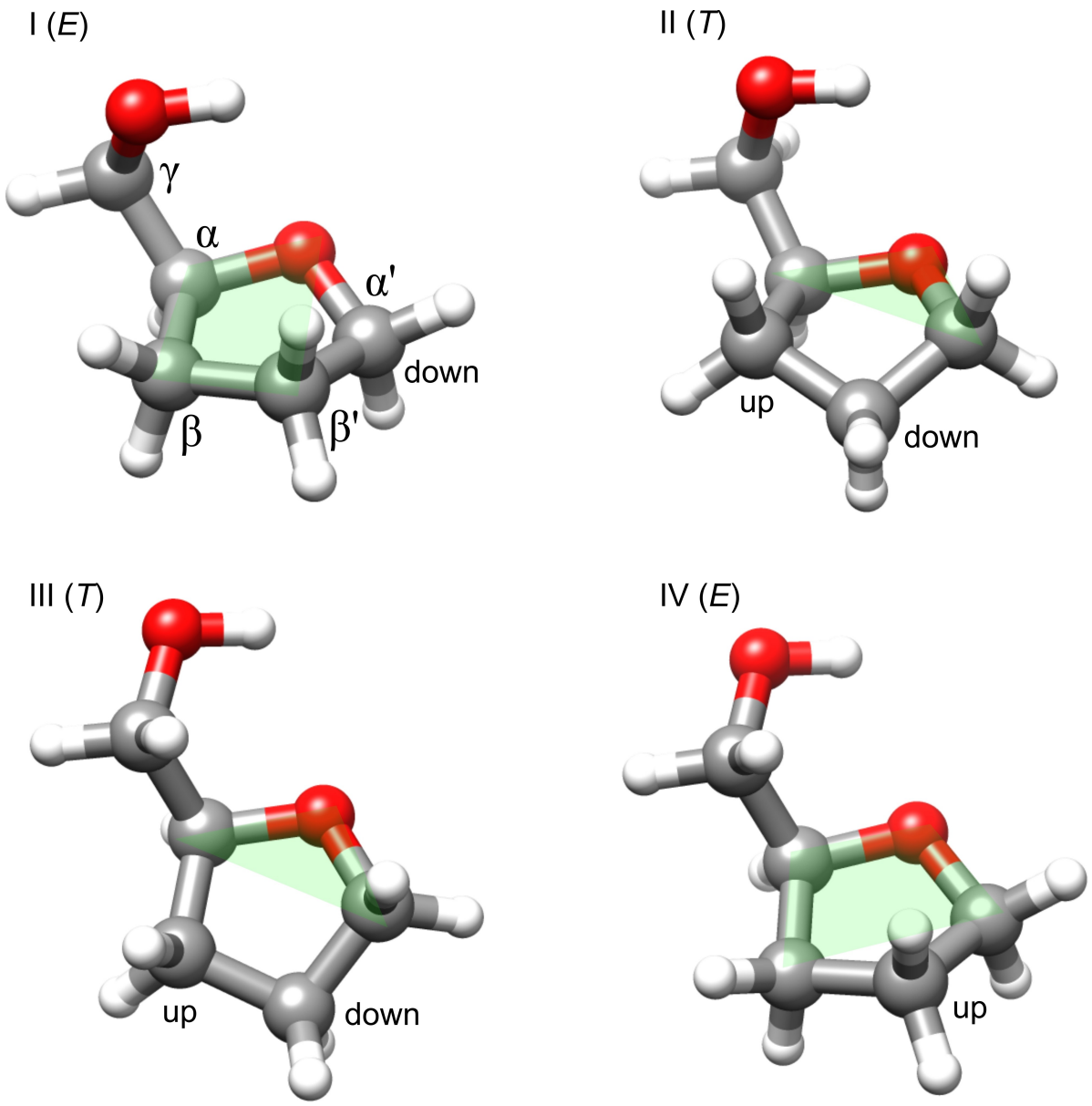

Figure 1. Four lowest energy geometries of THFA optimized at the B3LYP-D3(BJ)/aug-cc-pVTZ level of theory (see Table 1 for relative energies and spectroscopic parameters). Carbon, hydrogen, and oxygen atoms are depicted in grey, white, and red colours, respectively. The atoms that are puckered up or down from the plane formed by the coplanar adjacent atoms (sketched in green) are labeled to facilitate the visualization of the *envelope* (*E*) and *twist* (*T*) ring structures.

Owing to the advantages of rotational spectroscopy for determining molecular structures with high specificity and precision, we employed this technique to definitively establish the energy ordering of conformers of THFA for the first time. Using both chirped pulse and cavity-based Fourier transform microwave spectroscopies aided by quantum chemical calculations, we assigned transitions corresponding to two conformers of THFA with distinct ring structures. Confirmation of the geometries from detection of lines due to ^{13}C isotopologues allowed the influence of the CH_2OH moiety on the THF backbone to be evaluated through consideration of interconversion pathways and the noncovalent interactions responsible for conformer stability. Insights obtained regarding the specific conformations adopted by this important sugar analogue mark an important first step that can ultimately extend our understanding of the interactions of THFA and related derivatives in biologically relevant environments.

Results

Conformational Landscape

The study of the conformational space of THFA started with a conformational search for its local energy minima using Grimme's automated CREST[13] (conformer rotamer ensemble

sampling tool) procedure at the GFN2 level.[14] CREST produced a total of 18 possible structures for THFA, which were subsequently subjected to optimization and harmonic frequency calculations using the density functional theory (DFT) B3LYP-D3(BJ) method with the aug-cc-pVTZ basis set. This procedure identified 16 true energy minima for THFA within an energy window of 16.5 kJ mol^{-1}. As many conformers of THFA are very close in energy, we performed complementary single point energy calculations at the CCSD(T)/aug-cc-pVTZ level using their optimized geometric parameters from the B3LYP-D3(BJ) calculations. From these 16 structures, the four lowest conformers are expected to dominate the mixture at room temperature. In Figure 1, the geometries of these four most populated conformers are shown while their spectroscopic parameters are summarized in Table 1. The conformers are labeled in an increasing order of energy from I to IV based on their electronic energies from B3LYP-D3(BJ)/aug-cc-pVTZ. A full list of energies and spectroscopic parameters as well as the molecular geometries for all 16 minima of THFA is provided in the supplementary material.

Table 1. Calculated spectroscopic parameters for the four most stable conformers of THFA.

Parameter[a]	I(*E*)	II(*T*)	III(*T*)	IV(*E*)
A/MHz	4549	4903	5648	5201
B/MHz	2105	2024	1870	1958
C/MHz	1936	1806	1551	1632
$\lvert\mu_a\rvert$/Debye	1.8	1.9	2.8	3.0
$\lvert\mu_b\rvert$/Debye	0.4	0.8	1.0	1.1
$\lvert\mu_c\rvert$/Debye	0.9	0.5	1.0	0.3
$\triangle E$/kJ mol^{-1}	0.0	0.3	1.3	1.7
$\triangle E_{ZPE}$/kJ mol^{-1}	0.2	0.0	1.0	1.4
$\triangle G$/kJ mol^{-1}	0.1	0.0	0.0	1.0
$\triangle E_{CCSD(T)}$/kJ mol^{-1}	0.0	0.8	2.1	2.3

[a] Rotational constants (*A*, *B* and *C*), electric dipole moment components ($\lvert\mu_a\rvert$,$\lvert\mu_b\rvert$,$\lvert\mu_c\rvert$), relative electronic energy ($\triangle$E), relative electronic energy with zero-point corrections ($\triangle E_{ZPE}$) and relative Gibbs free energy ($\triangle$G) calculated at the B3LYP-D3(BJ)/aug-cc-pVTZ level. Relative electronic energy at the CCSD(T)/aug-cc-pVTZ level obtained through single-point energy calculations on the optimized geometries from B3LYP-D3(BJ)/aug-cc-pVTZ.

Conformers I and II are essentially isoenergetic (Table 1) and have the alcohol group in a *gauche* (*g*−) disposition relative to the oxygen heteroatom (OCCO ~−60°) differing only in the arrangement of heavy atoms in the ring backbone (Figure 1). Similarly, conformers III and IV are a higher energy pair, nearly isoenergetic, with the alcohol group in a *g*+ (OCCO ~+60°) orientation, but with different ring conformations. As in THF[3–8] and tetrahydro-2-furoic acid,[9] the five membered ring in THFA may adopt *envelope* (*E*) or *twist* (*T*) conformations. *E* ring structures (conformers I and IV) have four sequential coplanar atoms with the fifth puckered up or down with respect to the 4-atom plane. In the *T* configuration (II and III), there are three adjacent coplanar atoms, with the remaining two atoms being up or down from the 3-atom plane. The *g*+/*g*− orientation of the CH_2OH group and *E*/*T* ring geometries impart unique enough spectroscopic parameters (Table 1) for identification using FTMW methods.

Spectral Analysis and Structure Determination

As the rotational spectrum of THFA was not reported previously, the calculated values from Table 1 were used to guide the spectral analysis. Based on the distinct rotational constants, predicted relative energies at room temperature and sizeable dipole moment components, two sets of transitions consistent with the predicted patterns of conformers I(*E*) and III(*T*) were assigned (Figure 2). The assignment was subse-

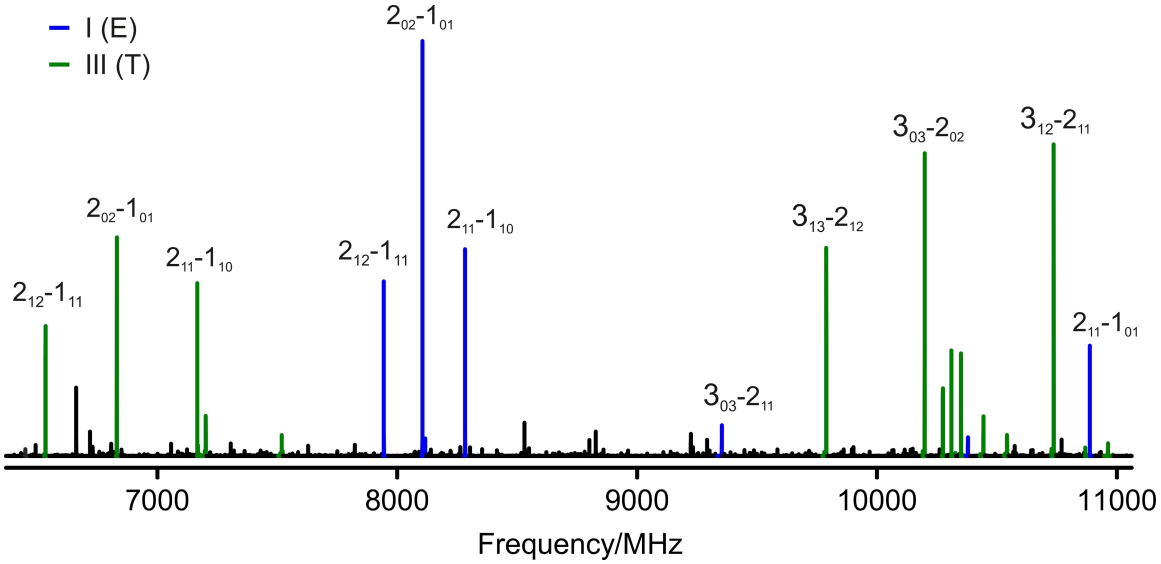

Figure 2. Section of the broadband cp-FTMW spectrum (1.5 M free induction decays) in the 6000–11000 MHz region highlighting select transitions for parent species of conformer I(*E*) and III(*T*) in blue and green, respectively. The labels refer to rotational quantum numbers $J'_{Ka'Kc'}-J''_{Ka''Kc''}$.

quently confirmed by observation of transitions due to singly substituted ^{13}C isotopologues in natural abundance whose intensities were ~1% of those observed for the parent species. Detecting transitions due to ^{13}C allowed accurate positions of carbon atoms in the ring to be determined to confirm whether the detected patterns correspond to structures with *E* or *T* ring geometries, or if they are highly averaged over a large amplitude motion.

The assigned transitions from the BF-FTMW instrument for conformers I(*E*) and III(*T*) were fitted using Pickett's SPFIT[15] program (Watson's S-reduced Hamiltonian[16] and I^r representation) to derive experimental ground state constants which are provided in Table 2. The full list of transition frequencies and fit residuals are given in the supplementary material. Using the experimentally-derived rotational constants from the parent and ^{13}C isotopologues (Table 2), the atomic coordinates for the five carbon atoms of conformers I(*E*) and III(*T*) were estimated by solving Kraitchman's equations[17] as implemented in Kisiel's KRA program.[18] The signs of the coordinates were inferred based on the calculated structures and these, along with their Costain[19] errors are summarized in the supplementary material. In Figure 3, the atom positions in the substitution structure (r_s) based on Kraitchman's equations are represented by magenta coloured spheres which are superimposed onto the equilibrium geometries (r_e) for comparison. The ground state effective geometries (r_0) were also derived by performing a least squares fit of the experimental moments of inertia upon variation of internal parameters using Kisiel's STRFIT program.[18] With knowledge about the vibration-rotation interaction constants (α) for the different vibrational modes of conformers I(*E*) and III(*T*) from anharmonic force field calculations at the B3LYP-D3(BJ)/aug-cc-pVTZ level and using the derived ground state rotational constants from Table 2, we obtained a set of semi-experimental (se) equilibrium rotational constants for the parent and ^{13}C species of conformers I(*E*) and III(*T*). By least-squares fitting the derived se equilibrium constants, a semi-experimental equilibrium geometry (r_{se}) was also derived for both conformers. The results from these three structural determination methods are summarized in Table 3.

Although conformers II(*T*) and IV(*E*) are also expected to be populated in the supersonic jet and have sizeable dipole moment components, no patterns of transitions consistent with these conformers were observed. The metastability of conformers II(*T*) and IV(*E*) will be discussed below.

Table 2. Ground state spectroscopic parameters derived for the parent and ^{13}C isotopologues of conformers I(*E*) and III(*T*) of THFA.

Parameter	I(*E*)	$^{13}C_{\alpha}$	$^{13}C_{\alpha'}$	$^{13}C_{\beta}$	$^{13}C_{\beta'}$	$^{13}C_{\gamma}$
A/MHz[a]	4548.39877(32)	4520.324(61)	4526.663(18)	4479.520(93)	4511.903(56)	4539.88(16)
B/MHz	2113.06886(14)	2106.35812(22)	2087.382600(82)	2109.10851(49)	2089.92821(21)	2085.63625(69)
C/MHz	1943.62851(13)	1943.05649(22)	1918.667430(82)	1931.14939(49)	1921.88702(21)	1921.79187(79)
D_J/kHz[b]	1.8161(25)	[1.816074621][f]	1.7560(26)	1.782(16)	[1.816074621]	1.746(23)
D_{JK}/kHz	−9.130(10)	[−9.12959648]	[−9.12959648]	[−9.12959648]	[−9.12959648]	[−9.12959648]
D_K/kHz	16.909(35)	[16.908775]	[16.908775]	[16.908775]	[16.908775]	[16.908775]
d_1/kHz	0.2111(18)	[0.21107349]	[0.21107349]	[0.21107349]	[0.21107349]	[0.21107349]
$\mu_a/\mu_b/\mu_c$[c]	y/y/y	y/n/n	y/n/n	y/n/n	y/n/n	y/n/n
N[d]	37	9	9	9	9	8
σ/kHz[e]	1.2	1.2	0.3	1.8	1.2	2.3
Parameter	III(*T*)	$^{13}C_{\alpha}$	$^{13}C_{\alpha'}$	$^{13}C_{\beta}$	$^{13}C_{\beta'}$	$^{13}C_{\gamma}$
A/MHz[a]	5647.50229(21)	5626.616(22)	5573.746(22)	5552.311(49)	5643.487(68)	5617.738(16)
B/MHz	1870.63564(12)	1868.87386(17)	1855.95105(17)	1864.37539(40)	1840.11351(49)	1854.39614(12)
C/MHz	1554.28250(10)	1553.33891(16)	1539.97271(17)	1542.51294(38)	1532.78883(48)	1542.18890(11)
D_J/kHz[b]	0.7419(15)	[0.741943615]	[0.741943615]	[0.741943615]	[0.741943615]	[0.741943615]
D_{JK}/kHz	−2.6602(66)	[−2.660190484]	[−2.660190484]	[−2.660190484]	[−2.660190484]	[−2.660190484]
D_K/kHz	12.771(29)	[12.771434]	[12.771434]	[12.771434]	[12.771434]	[12.771434]
d_1/kHz	−0.0352(14)	[−0.035236974]	[−0.035236974]	[−0.035236974]	[−0.035236974]	[−0.035236974]
d_2/kHz	−0.01990(83)	[−0.019871192]	[−0.019871192]	[−0.019871192]	[−0.019871192]	[−0.019871192]
$\mu_a/\mu_b/\mu_c$[c]	y/y/y	y/n/n	y/n/n	y/n/n	y/n/n	y/n/n
N[d]	48	10	9	10	10	10
σ/kHz[e]	1.0	1.2	1.2	2.8	3.4	0.8

[a] Rotational constants; [b] quartic centrifugal distortion constants; [c] electric dipole moment components ("y" if observed and "n" if not observed); [d] total number of lines (N) in the fit; [e] root-mean-square deviation of the fit (σ); [f]values in brackets were fixed to the values determined for the parent species. A complete list of calculated parameters at the B3LYP-D3(BJ)/aug-cc-pVTZ level for each conformer is provided as supplementary material for comparison.

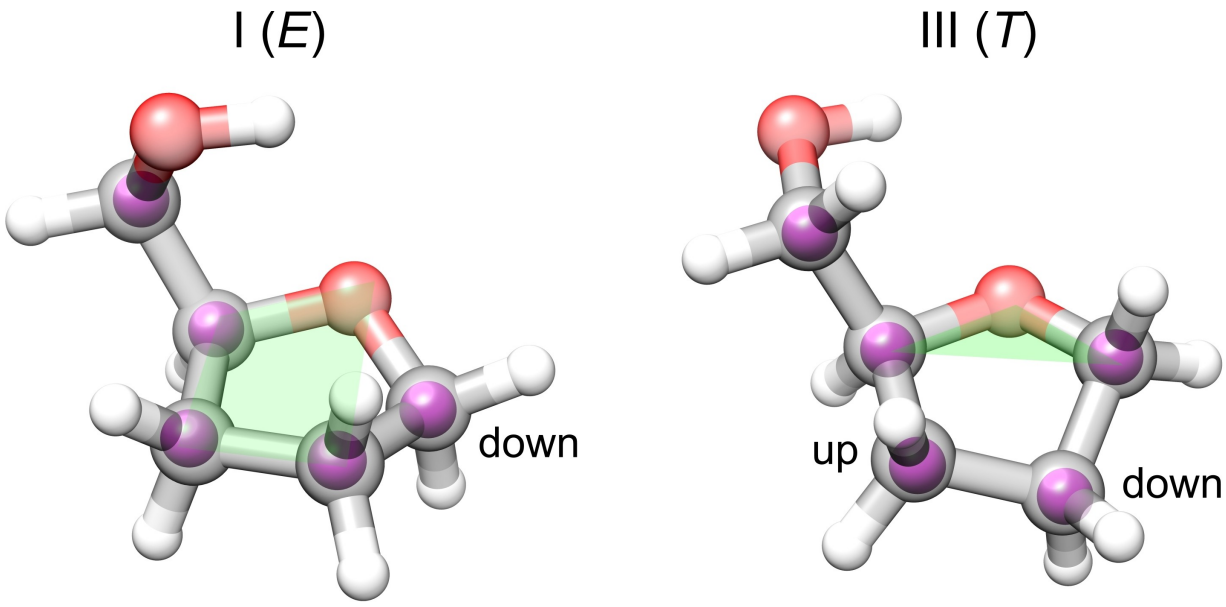

Figure 3. Comparison between equilibrium (r_e) and substitution (r_s) structures of THFA conformers I(*E*) and III(*T*). The magenta spheres represent the carbon atoms based on Kraitchman's coordinates which are superimposed onto the B3LYP-D3(BJ)/aug-cc-pVTZ geometries. The green planes represent the planes formed by the coplanar adjacent atoms to facilitate visualization. Kraitchman's atomic coordinates obtained along the *a*, *b* and *c* inertial axes with their corresponding uncertainties are provided in the supplementary material file.

Table 3. Ground state effective (r_0, *italic*), substitution (r_s, **bold**), semi-experimental equilibrium (r_{se}) and equilibrium (r_e) (B3LYP-D3(BJ)/aug-cc-pVTZ) structural parameters (bond lengths in Å, angles in deg) determined for the conformers of THFA.

Parameter	I(E)				II(T)	III(T)				IV(E)
	r_0	r_s	r_{se}	r_e	r_e	r_0	r_s	r_{se}	r_e	r_e
Bond length										
$C_{\beta'}$–$C_{\alpha'}$	1.519(6)	**1.531(3)**	1.512(13)	1.524	1.527	1.529(6)	**1.531(7)**	1.483(18)	1.523	1.523
C_{β}–$C_{\beta'}$	1.526(11)	**1.578(4)**	1.536(23)	1.538	1.530	1.529(8)	**1.523(4)**	1.512(26)	1.534	1.534
C_{α}–C_{β}	1.523(22)	**1.542(11)**	1.487(50)	1.547	1.526	1.557(8)	**1.560(6)**	1.540(26)	1.537	1.535
$C_{\gamma'}$–C_{α}	1.519(17)	**1.522(6)**	1.505(36)	1.518	1.520	1.510(10)	**1.512(6)**	1.457(34)	1.517	1.520
Bond angle										
C_{β}–$C_{\beta'}$–$C_{\alpha'}$	102.7(4)	**101.0(2)**	102.6(8)	102.33	101.98	101.6(2)	**100.9(2)**	103.4(6)	101.71	101.72
C_{α}–C_{β}–$C_{\beta'}$	104.5(6)	**102.7(3)**	104(1)	104.33	102.30	103.5(3)	**103.0(3)**	105(1)	103.56	103.30
$C_{\gamma'}$–C_{α}–C_{β}		**111.9(9)**		115.04	115.75		**113.9(4)**		113.71	113.41
Dihedral angle										
C_{α}–C_{β}–$C_{\beta'}$–$C_{\alpha'}$	−23.3(4)	**−24.1(3)**	−21.3(8)	−22.3	38.2	29.1(7)	**32(1)**	27(2)	31.0	−32.8
$C_{\gamma'}$–C_{α}–C_{β}–$C_{\beta'}$	−116.3(3)	**−116.8(5)**	−118.7(5)	−116.8	−150.3	−133.5(2)	**−134.8(8)**	−127.5(8)	−134.3	−98.8

Discussion

From the predicted DFT electronic relative energies in Table 1, the *g*− orientation of the CH_2OH group stabilizes conformers I-(*E*) and II(*T*) by at least ~1.0 kJ mol^{-1} over conformers III(*T*) and IV(*E*) with a *g*+ orientation while the ring conformation (*E* or *T*) within each pair has little effect on their energies. The relative energy differences between conformers I(*E*) and II(*T*) (~0.3 kJ mol^{-1}) and III(*T*) and IV(*E*) (~0.4 kJ mol^{-1}) at the DFT level are indeed so small that their stability ordering switches once ZPE corrections or Gibbs free energies are taken into consideration. The obtained energies for the four lowest energy conformers at the CCSD(T)/aug-cc-pVTZ level follow the same trend as those from the electronic energies at B3LYP-D3(BJ), but differences in the relative energy ordering are found for higher energy geometries (supplementary material). From these theoretical methods, it is impossible to determine the stability ordering of the conformers and definitively conclude which geometry corresponds to the global energy minimum of THFA.

On the other hand, as the predicted rotational constants for each conformer (Table 1) are unique and differ from other conformers by at least hundreds of MHz, they can be readily distinguished via rotational spectroscopy. When comparing the experimentally-derived constants and types of transitions

(Table 2) with the theoretical predictions (Table 1), it is evident that the spectrum reported herein arises from a combination of conformers I(*E*) and III(*T*). The excellent match between the experimental and theoretical parameters (largest deviation of 0.4% and 0.2% for I(*E*) and III(*T*), respectively) suggests that the effective ground state structures are not highly averaged over a large amplitude motion converting between *E* and *T* forms. Consequently, the experimental geometries (Table 3, Figure 3) derived from the spectroscopic parameters are in strong agreement with the equilibrium structures of conformers I(*E*) and III(*T*). In particular, the C_{α}–C_{β}–$C_{\beta'}$–$C_{\alpha'}$ and C_{γ}–C_{α}–C_{β}–$C_{\beta'}$ dihedral angles are key to distinguishing the conformers within each nearly isoenergetic pair and thus to unambiguously confirm that the ring backbones of the observed species are the *E*(I) and *T*(III) versions of the nearly isoenergetic pairs of $g-$ and $g+$ conformers, respectively. This deviates from the earlier gas phase electron diffraction study[10] which reported that the dominant structures are exclusively *T* ring configurations that most closely correlate with conformers II ($g-$ *T*) and III ($g+$ *T*) in Table 1. Although the authors had both HF and MP2/6-311++G** predictions to guide the data analysis, their conformer energy ordering followed the HF predictions. This favoured the assignment of the experimental data to a blend of *T* ring structures, a model which performed slightly better than other compositions based on the error from least squares fitting of the diffraction results. Interestingly, the relative energies from the MP2 calculations in reference [10] yield the same conformer energy ordering for the four most stable conformers as from our electronic energies based on B3LYP-D3(BJ) and CCSD(T) calculations in Table 1 and support the finding that *E* is the most stable form as conclusively determined in the present study from the assignment of distinct patterns of rotational transitions for six isotopologues of THFA.

For THFA, the experimental observation of transitions arising from conformers with *E* and *T* ring structures is intriguing as for both THF and tetrahydro-2-furoic acid for example, the conformational equilibrium is dominated by *E* ring configurations.[8,9] In tetrahydro-2-furoic acid,[9] 7 out of the 8 predicted total energy minima have *E* conformations, and the only *T* conformer is the sixth in order of energy being at least 8.4 kJ mol^{-1} less stable than the global minimum. In the rotational spectrum of tetrahydro-2-furoic acid, lines from the three lowest energy *E* conformers were seen.[9] The two lowest energy forms are the only ones that exhibit an intramolecular O···HO hydrogen bond and are stabilized by 4.3 kJ mol^{-1} (E + ZPE) in comparison to the third energy *E* conformer of the acid.

In the case of THFA here, the sp^3 hybridized carbon of the CH_2OH substituent provides additional flexibility and possible orientations of the OH group. The result is a larger number of energy minima (16), including stable conformers with *T* ring structures, such as conformer III(*T*) whose rotational fingerprint was experimentally observed. Apart from conformers I–IV (Figure 1 and Figure S1), no other conformer of THFA has the CH_2OH group in a $g-$ or $g+$ orientation, which is the favourable configuration for the formation of intramolecular hydrogen bonds stabilizing conformers I–IV by at least 6.4 kJ mol^{-1} (Table S1) in comparison to conformer V(*E*). For these conformers, the ring geometry (*E* versus *T*) has minimal influence on their relative energies as seen in Table 1 for the pairs of nearly isoenergetic minima which has contributed to the uncertainty regarding the structure of THFA in the literature before now. This is unique in comparison to the conformational equilibrium of tetrahydro-2-furoic acid[9] in which the two lowest energy conformers stabilized by a similar hydrogen bond, are separated by 1.8 kJ mol^{-1} due to small changes to the position of the ß-carbon in the ring and whether it is puckered down (global minimum) or up (second conformer).

Most of the 12 higher energy minima of THFA (Figure S1) can also be divided into pairs of conformers displaying the same CH_2OH orientation with *E/T* ring configurations and these pairs also remain nearly isoenergetic (e.g., IX(*E*) and X(*T*)). Notable exceptions include some pairs of conformers that instead differ in the *E* geometry itself (with different atoms puckered up) such as conformers XIV(*E*) and XV(*E*), and XIII(*E*) and XVI(*E*) which have energy differences as large as 2.3 kJ mol^{-1}. This suggests that the ring configuration plays a greater part in energy ordering of conformers with different *E* structures but is less distinct when comparing *E/T* geometries for a given CH_2OH orientation.

For THFA, although the relative energy differences between conformers I(*E*) and II(*T*) and also between III(*T*) and IV(*E*) are very small, the rotational spectrum unequivocally confirms that there is a clear energy ordering within these pairs as transitions due to conformers II(*T*) and IV(*E*) were not observed in the jet-cooled spectrum despite favourable dipole moments. This is consistent with conformational cooling which is known to occur in supersonic jet expansions when the energy barrier for the interconversion to a lower energy form is less than ~5 kJ mol^{-1}.[20] To explore this, we modeled potential relaxation pathways (B3LYP-D3(BJ)/aug-cc-pVTZ) and estimated the energy barriers between the nearly isoenergetic conformer pairs (Figure 4). This pathway essentially requires a pseudorotation motion linking the *E*↔*T* conformations when the CH_2OH group is $g-$ or $g+$. This can be visualized from the transition states associated with each pathway in Figure 4 in which the orientation of the OH group is maintained during the interconversion process. Based on the electronic energies of the optimized transition state geometries, small interconversion barriers of 1.7 kJ mol^{-1} and 1.5 kJ mol^{-1} are found between II(*T*)→I(*E*) and IV(*E*)→III(*T*), respectively, indicating that relaxation to the lower energy form of the ring is facile in the supersonic jet. Confirmation of conformational cooling can be derived from the observed spectral intensities of select rotational transitions with analogous quantum numbers from the BF-FTMW measurements and accounting for the electric dipole moments. From this, the estimated abundances of conformers I(*E*) and III(*T*) are ~65% and 35%, respectively. This is consistent with population transfer from II(*T*)→I(*E*) and IV(*E*)→III(*T*) in the molecular beam as the individual conformer populations at room temperature prior to the expansion based solely on the electronic energies at B3LYP-D(BJ) were calculated as: I(*E*)−33.3%, II(*T*)−29.8%, III(*T*)−19.7% and IV(*E*)−17.2%. The experimental abundances also agree well with the populations

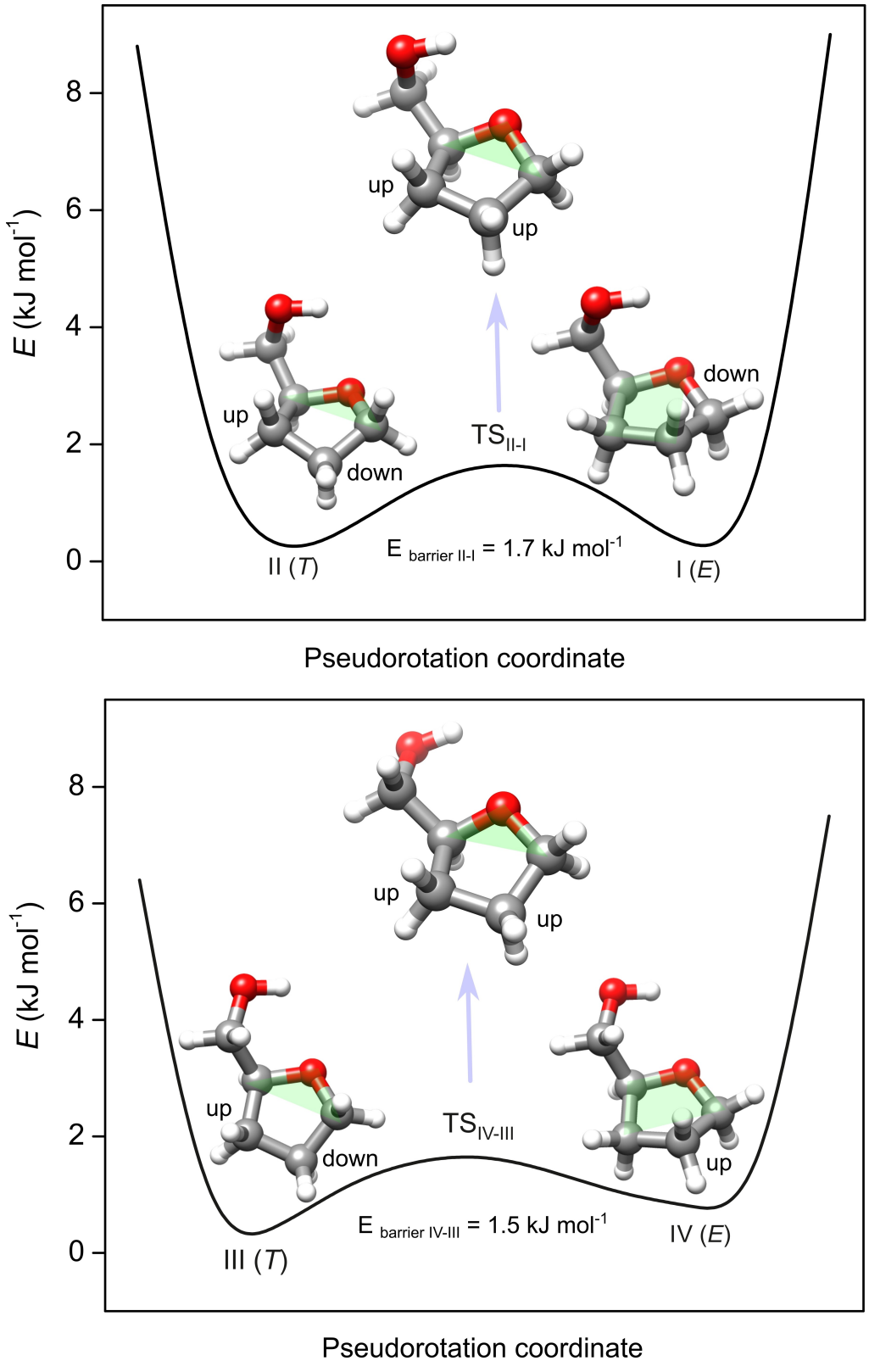

Figure 4. Pseudorotation interconversion pathways between conformers II(*T*)-I(*E*) (top) and IV(*E*)-III(*T*) (bottom) of THFA.

derived from the CCSD(T) energies: I(*E*)−39.1%, II(*T*)−28.9%, III(*T*)−16.6% and IV(*E*)−15.4%. If one considers the populations based on the DFT E+ZPE: I(*E*)−29.0%, II(*T*)−31.7%, III(*T*)−21.5% and IV(*E*)−17.8%, and G energies: I(*E*)−26.8%, II(*T*)−27.4%, III(*T*)−27.2% and IV(*E*)−18.6%, in which the ordering of conformers are different than those from the electronic energies,

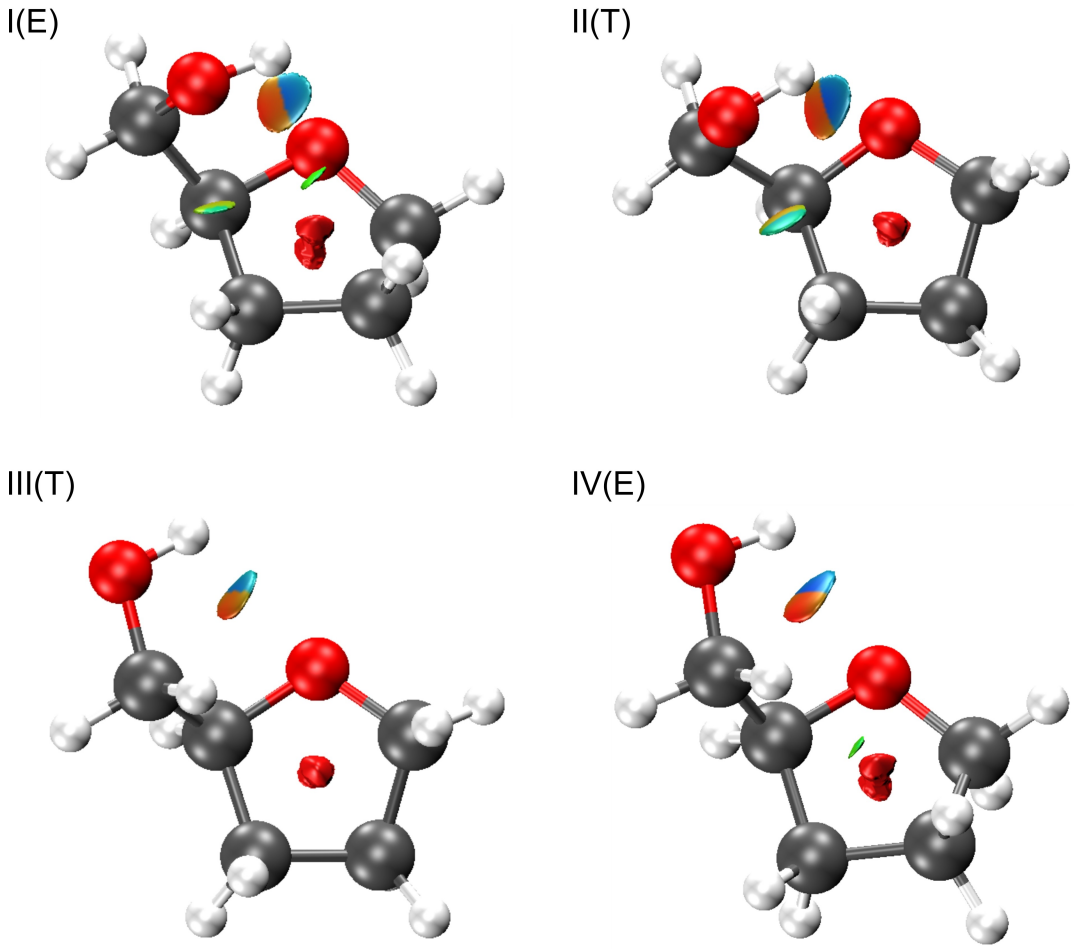

Figure 5. Non-covalent interaction (NCI) isosurfaces for the four most stable conformers of THFA. Blue, green and red coloured isosurfaces represent strong attractive, weak and strong repulsive interactions, respectively. The colour scheme is based on a $-0.02 < \rho < +0.02$ au scale with $s = 0.05$ au.

the derived spectral abundances still match the sum of the populations predicted for each isoenergetic pair, i.e. I(*E*) + II(*T*) and III(*T*) + IV(*E*). In tetrahydro-2-furoic acid,[9] for comparison, the energy barrier associated with the interconversion between pairs of the two lowest lying conformers was estimated to be ~5 kJ mol^{-1} which was sufficiently high that the higher energy *E* form persisted in the supersonic jet albeit partial relaxation to the lower energy *E* conformer was suggested to contribute to the lower than expected spectral intensities.

To finally understand the underlying effects responsible for the observed conformational stabilities, we carried out NCI analyses to visualize intramolecular interactions in the four most stable conformers of THFA. Based on the NCI isosurfaces shown in Figure 5, all four conformers are stabilized by an O···HO hydrogen bond characterized by the blue coloured isosurface between the ring O and the H atom of the hydroxyl group, as expected based on their *g*− and *g*+ orientations. The red colour portion of this isosurface represents repulsive interactions from the formation of a five-membered ring when the hydrogen bond is established. The same is true for the repulsive interactions within the THF unit which can be visualized in all conformers by the red isosurface in the middle of the ring. Apart from the dominant hydrogen bond, conformers I(*E*) and II(*T*) with a *g*− orientation of the CH_2OH group are further stabilized by weaker attractive contacts between the hydroxyl O and one H atom of the β-carbon (green coloured isosurfaces). Conformer I(*E*) also shows an additional long range interaction with one H on the β′-carbon (also green isosurface), which is most likely the reason of its slightly higher stability over II(*T*). When comparing the NCI plots of the higher energy pair of conformers III(*T*) and IV(*E*), a small green isosurface is visualized between one H of the substituent and one H of the β′-carbon in IV(*E*). Since green isosurfaces can represent both attractive and repulsive weak contacts in the NCI analysis, this interaction in IV(*E*) most probably corresponds to a repulsive interaction between these hydrogens (separated by 2.68 Å) which may be the reason of the higher stability of conformer III(*T*). Although in conformer III(*T*) the distance between the H of the γ-carbon that faces the ring and the H atom in the β-carbon is only 2.38 Å, no additional isosurfaces between these atoms appear in the NCI plot of III(*T*).

Conclusions and Outlook

The combined rotational spectroscopy and theoretical modeling approach reported here has definitively established the gas phase conformational landscape of THFA. In comparison to the THF ring which features four equivalent minima corresponding to envelope ring structures separated by a low pseudorotation barrier (50 cm^{-1}),[8] the presence of a CH_2OH substituent on the α-carbon of THF breaks the symmetry of the potential with respect to the ring geometry. This allows many low energy conformers for THFA, but two pairs of nearly isoenergetic conformers (I and II, III and IV) dominate the equilibrium. While it is a challenge for computational methods to conclude which conformer of each pair is lower in energy given their subtle structural differences, rotational spectroscopy allowed us to determine the most stable conformers of each pair (I and III with *E* and *T* ring structures, respectively). The observation of lines for conformers with both *E* and *T* ring configurations makes THFA unique in comparison to THF and tetrahydro-2-furoic acid for which only conformers with *E* configurations have been observed experimentally.

The absence of conformers II(*T*) and IV(*E*) is rationalized based on conformational cooling which is supported by the enriched experimental abundances of conformers I(*E*) and III(*T*) in the supersonic jet. Determining conformational abundances experimentally is also key for benchmarking relative energies obtained through quantum chemical calculations. For THFA, the observed conformational distribution matched better with those predicted based on the electronic energies from the B3LYP-D3(BJ) and CCSD(T) methods with the aug-cc-pVTZ basis sets. From NCI analysis, we determine that the higher stability of conformers I(*E*) and II(*T*) comes mainly from the *g*− orientation of the CH_2OH group which favours both primary O···HO and secondary CH···O hydrogen bonds. Furthermore, the higher stability of the lower energy conformer within each nearly isoenergetic pair may be a result of additional weaker long range contacts as suggested by the NCI plots. Collectively, the physical insights obtained in this work on the complex conformational landscape of this sugar analogue will contribute to a better understanding of related molecules built on the biochemically important THF unit. This is relevant for studies which aim to model processes happening in biological environments, such as interactions between water and carbohydrates in general.

Experimental Methods

The rotational spectrum of THFA was measured from 6–20 GHz using both a chirped-pulse (cp) and a cavity Balle-Flygare (BF) Fourier transform microwave spectrometer which have been described in detail previously.[21,22] THFA was purchased from Sigma-Aldrich Canada and used without further purification. As THFA (99% purity, bp: 178 °C) is a liquid at room temperature with low vapour pressure, to transfer the molecules into the gas phase, the sample was placed inside a glass bubbler through which Ne (200 kPa) was bubbled to serve as a carrier to deliver the sample to the spectrometer. In both experiments, the gas mixture (Ne + THFA) was expanded inside the high vacuum chamber of the spectrometers using a pulsed nozzle (1 mm orifice diameter, Series 9, Parker General Valve) to create a molecular beam in which the molecules are interrogated in isolation with no further collisions.

Initially, broadband spectra of THFA were collected from 6–18 GHz, in segments of 2 GHz each, using the cp-FTMW instrument from which the most intense transitions of the different species could be assigned. Final frequency measurements were performed using the cavity BF-FTMW spectrometer from 6–20 GHz which features higher resolution and sensitivity and allowed observation of less intense features and transitions at higher frequencies. In the BF-FTMW instrument, the spectral lines have widths of ~7 kHz (FWHM) and their positions are typically determined to within ~2 kHz. It is worth noting that each transition recorded in the BF-FTMW is split into two Doppler components as a result of the coaxial relationship of the molecular beam and resonator axis.

Computational Methods

A conformational search for the minima of THFA was performed using Grimme's CREST[13] (conformer rotamer ensemble sampling tool) procedure at the GFN2[14] level as implemented in the semiempirical xTB (extended tight binding) program. CREST generated a total of 18 possible structures for THFA. Next, all structures from CREST were optimized using the Gaussian 16 program[23] applying the dispersion-corrected density-functional theory (DFT) B3LYP[24] method with Becke-Johnson damping,[25,26] namely B3LYP-D3(BJ), in combination with Dunning's aug-cc-pVTZ[27] basis set. Harmonic frequency calculations were also carried out for the optimized structures at the same level of theory to confirm the nature of the stationary points, to obtain electronic energies with zero-point energy (ZPE) corrections, Gibbs free energies (G), and quartic centrifugal distortion constants. As the obtained energy differences between the conformers of THFA are very small and their energy orderings alter depending on if E, E + ZPE or G energies are considered, complementary single point calculations on the optimized DFT structures were carried out at the couple-cluster CCSD(T) level with the aug-cc-pVTZ basis set. For conformers I(*E*) and III(*T*) whose rotational fingerprints were observed in the spectrum, we also carried out anharmonic frequency calculations (B3LYP-D3(BJ)/aug-cc-pVTZ) for their parent and singly substituted ^{13}C species to obtain the vibration-rotation interaction constants (α) associated with each vibrational mode. This was needed for the determination of their semi-experimental equilibrium (r_{se}) structures.[28]

To understand conformational relaxation between different energy minima, interconversion pathways were modeled (B3LYP-D3(BJ)/aug-cc-pVTZ) and the geometries associated with the maxima on the interconversion pathways were subjected to optimization and frequency calculations. This is needed to guarantee that the maxima identified correspond to true transition states on the potential energy surface. Based on the transition state energies, barrier heights associated with the ring puckering motions were estimated. To identify and understand the intramolecular interactions in the most stable conformers of THFA, we carried out non-covalent interaction (NCI)[29] calculations using the NCIPLOT[30] program.

Supplementary Material

Appendix 1: Cartesian coordinates for the optimized structures of THFA at the B3LYP-D3(BJ)/aug-cc-pVTZ level; Appendix 2: Energetic and rotational parameters for the conformers of

THFA; Appendix 3: Transition frequencies and residuals for the observed species of THFA; Appendix 4: Spectroscopic parameters for the assigned conformers I(*E*) and III(*T*), Appendix 5: Kraitchman's atomic coordinates for conformers I(*E*) and III(*T*), Appendix 6: Vibration-rotation interaction constants (α) for the parent and ^{13}C species of conformers I(*E*) and III(*T*).

Acknowledgements

This research is funded by the Natural Sciences and Engineering Research Council of Canada (NSERC) through the Discovery Grant program (JvW) and the high-performance computing facility (GREX) provided by the University of Manitoba and Digital Research Alliance of Canada. W. G. D. P. S. also acknowledges support from a UMGF during his time at the University of Manitoba.

Conflict of Interests

The authors declare no conflict of interest.

Data Availability Statement

The data that support the findings of this study are available in the supplementary material of this article.

Keywords: conformational analysis · rotational spectroscopy · computational chemistry · hydrogen bonds · noncovalent interactions

[1] S. M. Bellm, J. D. Builth-Williams, D. B. Jones, H. Chaluvadi, D. H. Madison, C. G. Ning, F. Wang, X. G. Ma, B. Lohmann, M. J. Brunger, *J. Chem. Phys.* **2012**, *136*, 244301.
[2] S. Jin, Y. Hu, P. Wang, H. Zhan, Q. Lu, F. Liu, L. Sheng, *Phys. Chem. Chem. Phys.* **2018**, *20*, 7351–7360.
[3] D. G. Melnik, S. Gopalakrishnan, T. A. Miller, F. C. De Lucia, *J. Chem. Phys.* **2003**, *118*, 3589–3599.
[4] V. M. Rayón, J. A. Sordo, *J. Chem. Phys.* **2005**, *122*, 204303.
[5] A. Wu, D. Cremer, *Int. J. Mol. Sci.* **2003**, *4*, 158–192.
[6] R. Meyer, J. C. López, J. L. Alonso, S. Melandri, P. G. Favero, W. Caminati, *J. Chem. Phys.* **1999**, *111*, 7871–7880.
[7] A. H. Mamleev, L. N. Gunderova, R. V. Galeev, *J. Struct. Chem.* **2001**, *42*, 365–370.
[8] G. G. Engerholm, A. C. Luntz, W. D. Gwinn, D. O. Harris, *J. Chem. Phys.* **1969**, *50*, 2446–2457.
[9] F. Xie, X. Ng, N. A. Seifert, J. Thomas, W. Jäger, Y. Xu, *J. Chem. Phys.* **2018**, *149*, 224306.
[10] K. B. Borisenko, S. Samdal, I. F. Shishkov, L. V. Vilkov, *J. Mol. Struct.* **1998**, *448*, 29–41.
[11] P. Wang, Y. Hu, H. Zhan, J. Chen, S. Jin, W. Song, Y. Li, *Spectrochim. Acta Part A* **2017**, *185*, 63–68.
[12] P. Limão-Vieira, D. Duflot, M.-J. Hubin-Franskin, J. Delwiche, S. V. Hoffmann, L. Chiari, D. B. Jones, M. J. Brunger, M. C. A. Lopes, *J. Phys. Chem. A* **2014**, *118*, 6425–6434.
[13] S. Grimme, *J. Chem. Theory Comput.* **2019**, *15*, 2847–2862.
[14] C. Bannwarth, S. Ehlert, S. Grimme, *J. Chem. Theory Comput.* **2019**, *15*, 1652–1671.
[15] H. M. Pickett, *J. Mol. Spectrosc.* **1991**, *148*, 371–377.
[16] J. K. G. Watson in *Vibrational Spectra and Structure*, Vol. 6 (Ed.: James R. Durig), Elsevier, Amsterdam, **1977**, pp. 1–89.
[17] J. Kraitchman, *Am. J. Phys.* **1953**, *21*, 17–24.
[18] Z. Kisiel, *J. Mol. Spectrosc.* **2003**, *218*, 58–67.
[19] C. C. Costain, *Trans. Ameri. Cryst. Ass.* **1966**, *2*, 157–164.
[20] R. S. Ruoff, T. D. Klots, T. Emilsson, H. S. Gutowsky, *J. Chem. Phys.* **1990**, *93*, 3142–3150.
[21] G. Sedo, J. van Wijngaarden, *J. Chem. Phys.* **2009**, *131*, 044303.
[22] L. Evangelisti, G. Sedo, J. van Wijngaarden, *J. Phys. Chem. A* **2011**, *115*, 685–690.
[23] M. J. Frisch, G. W. Trucks, H. B. Schlegel, G. E. Scuseria, M. A. Robb, J. R. Cheeseman, G. Scalmani, V. Barone, G. A. Petersson, H. Nakatsuji, X. Li, M. Caricato, A. V. Marenich, J. Bloino, B. G. Janesko, R. Gomperts, B. Mennucci, H. P. Hratchian, et al., Gaussian 16, Revision C.01, Gaussian Inc., Wallingford CT, **2016**.
[24] A. D. Becke, *J. Chem. Phys.* **1993**, *98*, 5648–5652.
[25] A. D. Becke, E. R. Johnson, *J. Chem. Phys.* **2005**, *123*, 154101.
[26] S. Grimme, S. Ehrlich, L. Goerigk, *J. Comput. Chem.* **2011**, *32*, 1456–1465.
[27] D. E. Woon, T. H. Dunning, *J. Chem. Phys.* **1993**, *98*, 1358–1371.
[28] M. Melosso, S. Alessandrini, L. Spada, A. Melli, X. Wang, Y. Zheng, C. Duan, J. Li, W. Du, Q. Gou, L. Bizzocchi, L. Dore, V. Barone, C. Puzzarini, *Phys. Chem. Chem. Phys.* **2023**, *25*, 31281–31291.
[29] E. R. Johnson, S. Keinan, P. Mori-Sánchez, J. Contreras-García, A. J. Cohen, W. Yang, *J. Am. Chem. Soc.* **2010**, *132*, 6498–6506.
[30] J. Contreras-García, E. R. Johnson, S. Keinan, R. Chaudret, J.-P. Piquemal, D. N. Beratan, W. Yang, *J. Chem. Theory Comput.* **2011**, *7*, 625–632.

Manuscript received: March 17, 2024
Revised manuscript received: April 18, 2024
Accepted manuscript online: April 18, 2024
Version of record online: ■■, ■■

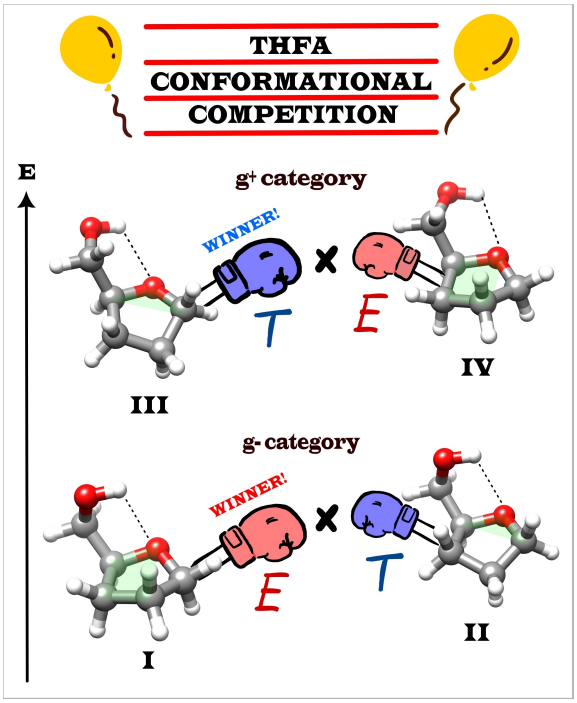

*W. G. D. P. Silva, J. van Wijngaarden**

1 – 11

Disentangling the Conformational Space and Structural Preferences of Tetrahydrofurfuryl Alcohol Using Rotational Spectroscopy and Computational Chemistry

THFA is dominated by two pairs of nearly-isoenergetic conformers with different ring structures: envelope(E) or twist(T). When CH_2OH lies *gauche*−(OCCO = −60°) to the ring, the *E* conformer is favoured, while the opposite happens for the *g* + pair, as confirmed by observing rotational transitions from conformers I(E) and III(T) experimentally.